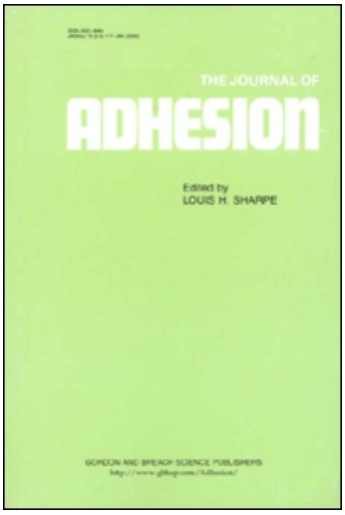

The Journal of Adhesion
Publication details, including instructions for authors and subscription information:
http://www.informaworld.com/smpp/title~content=t713453635

Scarf Repair Joints in Carbon Fibre Reinforced Plastic Strips

J. P. H. Webber[a]
[a] Department of Aeronautical Engineering, University of Bristol, England

To cite this Article Webber, J. P. H.(1981) 'Scarf Repair Joints in Carbon Fibre Reinforced Plastic Strips', The Journal of Adhesion, 12: 4, 257 — 281
To link to this Article: DOI: 10.1080/00218468108071206
URL: http://dx.doi.org/10.1080/00218468108071206

J. Adhesion, 1981, Vol. 12, pp. 257–281
0021–8464/81/1204–0257 $06.50/0

Printed in Great Britain

Scarf Repair Joints in Carbon Fibre Reinforced Plastic Strips

J. P. H. WEBBER

Department of Aeronautical Engineering, University of Bristol, BS8 1TR, England.

(*Received December 12, 1980; in final form February 15, 1981*)

Various theoretical models are developed for scarf joint repairs in unidirectional carbon fibre reinforced plastic strips subjected to a tensile load. For the type of joint where the fibres of both the original and repair materials (the adherends) are aligned along the longitudinal axis of the joint (a dry/dry joint), a uniform shear stress is predicted in the adhesive layer. When the repair material is laid directly on to the scarf surface with the fibres inclined to the longitudinal axis (a wet/dry joint), it is shown that the degree of shear stress uniformity is a function of the scarf angle, but reaches a uniform state at slopes smaller than 1 : 30 when the joint stresses can be calculated very simply.

The theoretical work is supported by tests on a number of joints of both types. The test results show that the dry/dry joints are more efficient than the wet/dry joints, and that it is possible to achieve joint efficiencies at failure, under a static load, in the region of 90% with slopes less than or equal to about 1 : 65.

NOTATION

$a'_{11}, a'_{13}, a'_{33}$	defined by equation (15)
c	defined by equation (12)
d	distance between tapered ends (Figure 1(a))
E	Young's modulus
$f(x)$	defined by equations (23) and (26)
G	shear modulus
$g(x)$	defined by equations (24) and (27)
h	thickness of strip
$h_{1,2}$	thickness of material (1), (2) at x
l	length of scarf joint
n	number of divisions in joint for finite difference approximation
P_0	applied tensile load per unit width
$P_{1,2}$	tensile load per width in material (1), (2)
S	shear strength
Δu	relative displacement across adhesive layer
X, Y, Z	local co-ordinates with X in fibre direction; also tensile strengths in associated directions
x, y, z	joint co-ordinates

α scarf angle
β angle between X and x co-ordinates
$\gamma_1, \gamma_2, \gamma_3$ defined by equations (19) and (21)
ε direct strain
ν Poisson's ratio
σ direct stress
σ_0 applied stress
σ_A direct stress in adhesive layer (normal to scarf plane)
τ_A shear stress in adhesive layer (parallel to scarf plane)

Suffixes

1 material 1 (original)
2 material 2 (repair)
A adhesive
i ith division

1 INTRODUCTION

In present-day sailplanes, the main spar tension and compression caps are often in the form of rectangular strips made from unidirectional glass or carbon fibre reinforced plastic materials. When damaged in one particular spot, it is envisaged that a satisfactory repair could be made in the form of a scarf joint, wherein the original damaged material is cut away at an angle, and new material is inserted as shown diagrammatically in Figures 1(a) and 1(b). The essential difference between these two figures can be seen within the circled regions. In Figure 1(a), the fibre tows, which constitute the repair material, are laid on to the scarf slope in the wet condition so that in this region the fibres run parallel to the scarf angle. In Figure 1(b), the repair material has been cut out from a cured (dry) strip of unidirectional material and has then been glued on to the angled surface. This is known as a dry/dry joint.

Now it is fairly well known that for a pure scarf joint between like elastic isotropic adherends[1] there is no stress concentration set up in the joint. (However, there is the slight problem of a non-vanishing shear stress at the ends of the joint where, in fact, there is an adhesive-to-air surface which is incapable of sustaining such a stress, but in cases where the adhesive layer is very thin, compared with the adherends, this effect is considered to be small and has been neglected in the present study. Furthermore, local plastic deformation of the adhesive usually eliminates this as a source of failure.) It would seem then that even when the adherends are in the form of orthotropic carbon fibre materials, then providing they are the same, there should be no stress concentrations. This will not be the case for the wet/dry joint shown in Figure 1(a) since the effect of laying the fibres along the slope will reduce the major Young's modulus of the material in the longitudinal direction thereby making the adherends, effectively, different materials.

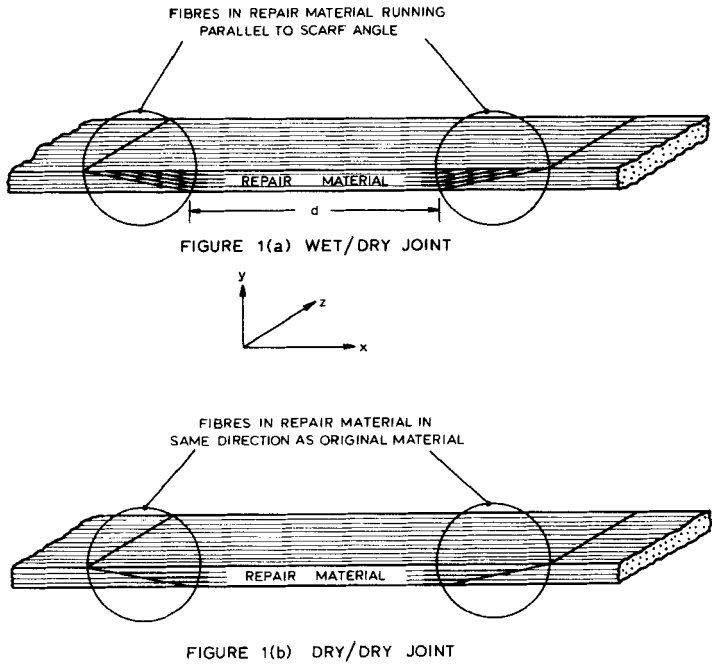

FIGURE 1 Scarf joints in fibre reinforced plastic strips.

However, for very small scarf angles there should be little difference between the two types of joints and the main objective behind this work is to investigate, both theoretically and experimentally, differences in structural behaviour which might exist between the two. The work has been limited to joints subjected to a uniform tension stress and although, in principle, it should be possible to apply the results to joints in compression, in practice the joints may fail at lower loads due to local instability effects, and non-linear material stress-strain properties.[2]

In the theoretical work, the emphasis is placed on determining the shear stress distribution in the adhesive layer along the scarf surface, and the tensile stresses in the carbon fibre material, for various scarf angles. The results show that in both the cases of the wet/dry and dry/dry joints, it should be possible to design joints which are devoid of stress concentrations and which would give high structural efficiencies.

The theoretical work is supported by tests on a number of scarf joint specimens, although they showed that the dry/dry joint could be made to give a much higher efficiency than the wet/dry joint. This is thought to be due to the difficulty experienced in compacting the wet fibre tows when being laid along the inclined scarf surface.

2 THEORY

Erdogan and Ratwani[3] discuss stresses in bonded joints and give an analysis for a smoothly tapered (or scarf) joint. The adhesive layer is treated as an elastic medium acting basically as a combination of a shear medium and separate tension springs. The analysis given here is based on this, but is extended to take into account the alignment of the repair material along the scarf slope, for the wet/dry joint. (Figure 1 (a)).

Consider a side view of the joint (the x, y plane of Figure 1), as shown in Figure 2. The thickness h is taken to be small compared with the dimensions in the x and z directions and the stresses in the thickness direction are neglected in materials (1) and (2). Furthermore, the stresses which do exist in materials (1) and (2) are assumed not to vary with y.

Figure 2 also shows a free body diagram of an element in material (2) of length dx, bounded by the free surface at the top, and the inclined scarf slope at the bottom. τ_A and σ_A are the shear stress and normal stress in the thin adhesive layer and σ_{x_2} is the tensile stress in material (2) at x. Taking unit breadth of strip in the "z" direction we can resolve forces in the x and y directions to give

$$\frac{\mathrm{d}}{\mathrm{d}x}(x\sigma_{x_2} \tan \alpha) = \sigma_A \tan \alpha + \tau_A \tag{1}$$

and

$$\sigma_A = \tau_A \tan \alpha \tag{2}$$

Noting that $x\sigma_{x_2} \tan \alpha = P_2$ (the end load per unit width in material (2)) then Eq. (1) becomes:

$$\frac{\mathrm{d}}{\mathrm{d}x}(P_2) = \sigma_A \tan \alpha + \tau_A \tag{3}$$

Eliminating σ_A from Eqs (2) and (3) gives:

$$\frac{\mathrm{d}P_2}{\mathrm{d}x} = \tau_A(\tan^2 \alpha + 1) \tag{4}$$

Now, a very simple solution to the problem can be obtained if we assume that P_2 varies as the cross-sectional area of material (2). Then

$$P_2 = \frac{P_0 x}{h} \tan \alpha \tag{5}$$

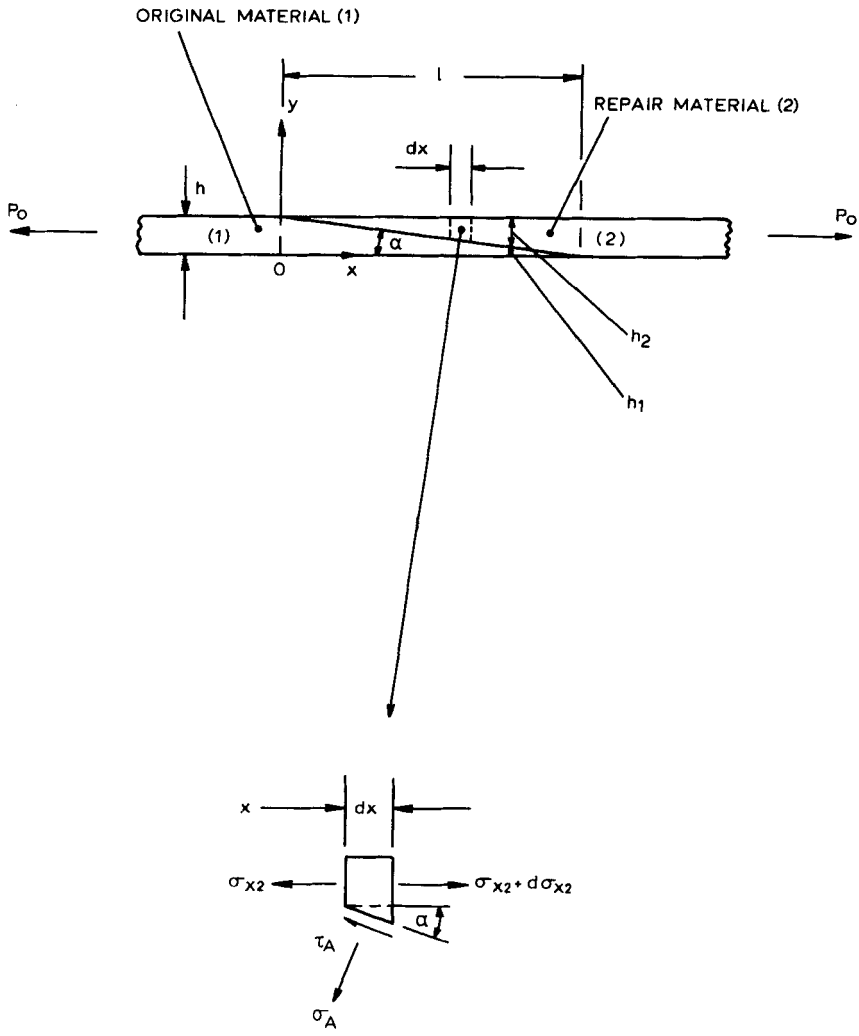

FIGURE 2 Geometry of scarf joint and free body diagram.

and

$$\frac{dP_2}{dx} = \frac{P_0}{h} \tan \alpha$$

Using this result in Eq. (4) gives:

$$\tau_A = \left(\frac{P_0}{h}\right) \sin \alpha \cos \alpha \tag{6}$$

which agrees with Eq. (2.2) of Ref. 1. Note that this equation could also have been derived more directly from the assumption that τ_A and σ_A are constant.

However, this simple solution, of course, depends on the assumption that P_2 varies linearly with "x" and this may not be so in practice, particularly in the case of the wet/dry joint. Note that the solution, so far, does not depend on material or adhesive mechanical properties and that it has been obtained entirely from conditions of load equilibrium.

In order to obtain a more satisfactory solution, we have to introduce strain-displacement and stress-strain equations, and use these with Eq. (4) to solve for P_2. For the adhesive layer, Erdogan and Ratwani[3] show that the relative normal and tangential displacements across the adhesive thickness h_A are given by

$$\Delta u_n = \frac{h_A}{E_A}\sigma_A \quad \text{and} \quad \Delta u_t = \frac{h_A}{G_A}\tau_A \tag{7}$$

with the assumption that the adhesive layer acts, separately, as tension springs and a shear medium. The relative displacement component in the x direction then becomes:

$$\Delta u_x (= u_{x_2} - u_{x_1}) = \Delta u_t \cos\alpha + \Delta u_n \sin\alpha$$

or using Eqs (7) and (2) this becomes

$$u_{x_2} - u_{x_1} = h_A\left(\frac{1}{G_A} + \frac{\tan^2\alpha}{E_A}\right)\tau_A \cos\alpha \tag{8}$$

Differentiating with respect to x gives

$$\frac{du_{x_2}}{dx} - \frac{du_{x_1}}{dx} = h_A\left(\frac{1}{G_A} + \frac{\tan^2\alpha}{E_A}\right)\cos\alpha\frac{d\tau_A}{dx} \tag{9}$$

Now u_{x_1} is the displacement in material (1) at x, and is assumed to be uniform across the thickness of the material, in the y direction. Thus du_{x_1}/dx represents the direct strain in material (1) at x so that Eq. (9) may be written:

$$\varepsilon_{x_2} - \varepsilon_{x_1} = h_A\left(\frac{1}{G_A} + \frac{\tan^2\alpha}{E_A}\right)\cos\alpha\frac{d\tau_A}{dx} \tag{10}$$

Combining this with Eq. (4) gives

$$\frac{d^2P_2}{dx^2} = \frac{1}{c}(\varepsilon_{x_2} - \varepsilon_{x_1}) \tag{11}$$

where

$$c = \frac{h_A\cos\alpha}{(1+\tan^2\alpha)}\left[\frac{1}{G_A} + \frac{\tan^2\alpha}{E_A}\right] \tag{12}$$

a constant which is dependent only on the scarf angle, the adhesive thickness and its mechanical properties.

In order to proceed with the solution to Eq. (11) we have to introduce the stress-strain equations for materials (1) and (2) so that the right hand side of Eq. (11) can be obtained in terms of P_2 through the overall force equilibrium equations,

$$P_2 = \sigma_{x_2} x \tan \alpha \quad \text{and} \quad P_0 - P_2 = P_1 = \sigma_{x_1}(h - x \tan \alpha) \tag{13}$$

Bearing in mind that the materials are orthotropic and that we need to be able to include the effect of the inclined fibres for the wet/dry joint (Figure 1(a)) we shall, for the moment, take the stress-strain equations in their most general form,[4] but, in accordance with the initial assumptions, neglect y-wise stresses and strains and shear effects. This gives:

$$\begin{aligned} \varepsilon_x &= a'_{11}\sigma_x + a'_{13}\sigma_z \\ \varepsilon_z &= a'_{13}\sigma_x + a'_{33}\sigma_z \end{aligned} \tag{14}$$

where

$$\begin{aligned} a'_{11} &= \frac{\cos^4 \beta}{E_X} + \left(\frac{1}{G_{XY}} - \frac{2\nu_{XY}}{E_X}\right)\sin^2 \beta \cos^2 \beta + \frac{\sin^4 \beta}{E_Y} \\ a'_{13} &= -\left(\frac{\nu_{YZ}}{E_Y}\sin^2 \beta + \frac{\nu_{ZX}}{E_Z}\cos^2 \beta\right) \\ a'_{33} &= \frac{1}{E_Z} \end{aligned} \tag{15}$$

In Eq. (15), the XYZ co-ordinates are the main orthotropic axes of the fibre reinforced materials with X in the fibre direction, whilst β is the angle of inclination of the X axis to the x axis. Thus for material (1),

$$\beta = 0; \quad X \equiv x; \quad Y \equiv y \quad \text{and} \quad Z = z$$

and for material (2), for the wet/dry joint only, $\beta = \alpha$ with Z coincident with z.

Now Eq. (14) contains stresses and strains in the transverse z direction and it is reasonable to make certain assumptions with regard to these particular stresses and strains. In the work which follows, as in Ref. 3, we shall either assume that the total force in the z direction is zero or that the z-wise strains are zero. The first assumption is consistent with a long specimen where the joint is not constrained by the ends, and the second assumption is consistent with a short specimen with clamped ends, which give rise to constraint in the z-wise direction. Thus in the first case, we put

$$h_1 \sigma_{z_1} + h_2 \sigma_{z_2} = 0 \tag{16}$$

but with the additional condition

$$\varepsilon_{z_1} = \varepsilon_{z_2} \tag{17}$$

Eqs (16) and (17) lead to the condition that

$$\sigma_{z_1} = \frac{a'_{13(2)}\sigma_{x_2} - a'_{13(1)}\sigma_{x_1}}{a'_{33(1)} + \dfrac{h_1}{h_2}a'_{33(2)}} = \frac{a'_{13(2)}\sigma_{x_2} - a'_{13(1)}\sigma_{x_1}}{\gamma_1(x)} \tag{18}$$

where

$$\gamma_1(x) = a'_{33(1)} + \frac{h_1}{h_2}a'_{33(2)} = a'_{33(1)} - a'_{33(2)} + \frac{a'_{33(2)}h}{x\tan\alpha} \tag{19}$$

since

$$\frac{h_1}{h_2} = \frac{h}{x\tan\alpha} - 1$$

In Eqs (18) and (19) the suffixes (1) and (2) apply to materials (1) and (2) respectively. Eq. (18) is now used in the first of Eqs (14) to yield

$$\varepsilon_{x_2} - \varepsilon_{x_1} = \frac{1}{\gamma_1(x)}[\gamma_2(x)\sigma_{x_1} + \gamma_3(x)\sigma_{x_2}] \tag{20}$$

where

$$\gamma_2(x) = (a'_{13(2)}a'_{13(1)} - a'_{11(1)}a'_{33(2)})\left(\frac{h}{x\tan\alpha} - 1\right) - a'_{11(1)}a'_{33(1)} + a'^2_{13(1)} \tag{21}$$

and

$$\gamma_3(x) = (a'_{33(2)}a'_{11(2)} - a'_{13(2)}a'_{13(2)})\left(\frac{h}{x\tan\alpha} - 1\right) - a'_{13(1)}a'_{13(2)} + a'_{11(2)}a'_{33(1)}$$

But σ_{x_1} and σ_{x_2} are given in terms of P_0 and P_2 from Eq. (13), so that Eq. (20) becomes

$$\varepsilon_{x_2} - \varepsilon_{x_1} = P_2\left\{\frac{\gamma_3(x)}{\gamma_1(x)x\tan\alpha} - \frac{\gamma_2(x)}{\gamma_1(x)[h - x\tan\alpha]}\right\} + \frac{\gamma_2(x)P_0}{\gamma_1(x)[h - x\tan\alpha]} \tag{21a}$$

Substituting this expression into Eq. (11) gives the final governing differential equation for the problem,

$$\frac{d^2P_2}{dx^2} - f(x)P_2 = g(x) \tag{22}$$

where

$$f(x) = \frac{1}{c}\left\{\frac{\gamma_3(x)}{\gamma_1(x)\,x\,\tan\alpha} - \frac{\gamma_2(x)}{\gamma_1(x)[h - x\,\tan\alpha]}\right\} \tag{23}$$

and

$$g(x) = \frac{P_0}{c}\left\{\frac{\gamma_2(x)}{\gamma_1(x)[h - x\,\tan\alpha]}\right\} \tag{24}$$

The solution of Eq. (22) for P_2, subject to the boundary conditions $P_2(0) = 0$ and $P_2(h/\tan\alpha) = P_0$, solves the complete problem, since all other quantities such as σ_{x_1}, σ_{x_2}, τ_A and σ_A can then be obtained.

We now develop the second model in which the z-wise strains are put equal to zero, *i.e.* $\varepsilon_{z_1} = \varepsilon_{z_2} = 0$. In this case Eq. (14) allows us to write

$$\varepsilon_{x_2} - \varepsilon_{x_1} = \sigma_{x_2}\left(a'_{11(2)} - \frac{a'^2_{13(2)}}{a'_{33(2)}}\right) - \sigma_{x_1}\left(a'_{11(1)} - \frac{a'^2_{13(1)}}{a'_{33(1)}}\right) \tag{25}$$

and we again obtain Eq. (22) but with

$$f(x) = \frac{1}{c}\left\{\frac{1}{x\,\tan\alpha}\left(a'_{11(2)} - \frac{a'^2_{13(2)}}{a'_{33(2)}}\right) + \frac{1}{(h - x\,\tan\alpha)}\left(a'_{11(1)} - \frac{a'^2_{13(1)}}{a'_{33(1)}}\right)\right\} \tag{26}$$

and

$$g(x) = \frac{P_0}{c(h - x\,\tan\alpha)}\left\{\frac{a'^2_{13(1)}}{a'_{33(1)}} - a'_{11(1)}\right\} \tag{27}$$

To summarise, at this stage, we see that it is possible to consider four different models, A, B, C and D depending on whether or not we have a dry/dry or wet/dry joint and upon the conditions of zero z-wise strain or force. The various models are defined as follows, and details of the appropriate equations to use in each case are given in Table I.

Model A—Dry/Dry; $\varepsilon_{z_1} = \varepsilon_{z_2} = 0$

Model B—Dry/Dry; z-wise force = 0 and $\varepsilon_{z_1} = \varepsilon_{z_2}$

Model C—Wet/Dry; $\varepsilon_{z_1} = \varepsilon_{z_2} = 0$

Model D—Wet/Dry; z-wise force = 0 and $\varepsilon_{z_1} = \varepsilon_{z_2}$

TABLE I

Summary of theoretical models

Model	Type of joint	Z-wise condition	Equation No. for $f(x)$	Equation No. for $g(x)$	$a'_{11(1)}$	$a'_{13(1)}$	$a'_{33(1)}$	$a'_{11(2)}$	$a'_{13(2)}$	$a'_{33(2)}$
A	dry/dry	$\varepsilon_{z_1} = \varepsilon_{z_2} = 0$	(26)	(27)	$\frac{1}{E_X}$	$-\frac{\nu_{ZX}}{E_Z}$	$\frac{1}{E_Z}$	$\frac{1}{E_X}$	$-\frac{\nu_{ZX}}{E_Z}$	$\frac{1}{E_Z}$
B	dry/dry	Force = 0 $\varepsilon_{z_1} = \varepsilon_{z_2}$	(23)	(24)	← as model A →					
C	wet/dry	$\varepsilon_{z_1} = \varepsilon_{z_2} = 0$	(26)	(27)	← as model A →			see Eqns (15) ← with $\beta = \alpha$ →		
D	wet/dry	Force = 0 $\varepsilon_{z_1} = \varepsilon_{z_2}$	(23)	(24)	← as model A →			← as model C →		

In fact, it can be shown that the $f(x)$ and $g(x)$ functions for both Models A and B are identical, providing materials (1) and (2) are the same. This is not the case for Models C and D where small differences occur in the expressions for $f(x)$ and $g(x)$.

3 THEORETICAL RESULTS

The problem now is to solve Eq. (22) for the variable $P_2(x)$. Because of the nature of the expressions for $f(x)$ and $g(x)$, in this equation, it has not been possible to find an analytical solution, and recourse was made to the finite difference method.[5]† The scarf joint is divided up into a large number of divisions, with the distance between each division equal to s. If, at a typical division, say i, the values of $P_2(x)$, $f(x)$ and $g(x)$ are $P_{2(i)}$, f_i and g_i respectively, then it can be shown that the central finite difference form for Eq. (22) is

$$P_{2(i+1)} + P_{2(i-1)} - (2 - s^2 f_i) P_{2(i)} - h^2 g_i P_{2(i)} = 0 \tag{28}$$

with the boundary conditions

$$P_{2(0)} = 0; \quad P_{2(n)} = P_0$$

where n is the total number of divisions.

Eq. (28) gives n simultaneous linear equations for P_i. These equations were solved on a digital computer using double-precision arithmetic in order to avoid rounding errors.

As a first check on the accuracy of the solution, some results are obtained for an example give in Ref. 3. These are for an aluminium strip bonded to an

† In fact, this method of solution is used by Thamm[6] when considering the problem of lap joints with partially tapered adherends.

TABLE II

Values of P_2 for comparison with Figure 6b of Ref. 3

x (in)	0.225	0.450	0.675	0.900	1.125	1.35	1.575	1.8
$\frac{P_2}{P_0}$	0.296	0.496	0.640	0.747	0.831	0.899	0.954	1.00
$\frac{P_2}{P_0}$ (Ref. 3)		0.501		0.752		0.895		1.003

orthotropic boron-epoxy composite strip and are shown in Figure 6 of this reference. The variation of P_2 (Ref. 3 uses ϕ) with x is shown in Figure 6(b), Ref. 3, and these values can be seen to compare very well with those given in Table II, from the present solution, using 40 divisions in the finite difference analysis. In fact, this number of divisions was used throughout, and was found to give results of sufficient accuracy.

The results for carbon fibre strips are based on the following values for the joint geometry and mechanical properties, with the value of E_X being representative of material supplied by Slingsby Engineering Ltd. as discussed in Section 4. Also, the value of E_A was obtained from the same source. Other values quoted are based on Ref. 2 and related tests, and are thought to be representative of the Slingsby material.

$E_X = 108 \times 10^3 \text{N/mm}^2$; $E_Y = 8 \times 10^3 \text{N/mm}^2$
$E_Z = 8 \times 10^3 \text{N/mm}^2$
$\nu_{XY} = 0.335$; $\nu_{ZX} = 0.024$
$\nu_{YZ} = 0.3$
$G_{XY} = 1000$, 4000 and 6000 N/mm^2
$E_A = 2670 \text{ N/mm}^2$; $G_A = 1000 \text{ N/mm}^2$
$h_A = 0.001$, 0.005 and 0.05 mm
$h = 1$ mm
Scarf slopes 1 : 5 to 1 : 100

For models A and B the numerical results showed that the variation of P_2 with x was always linear, giving a uniform shear stress in the glue layer. This was found to be so for all scarf angles and was found not to be dependent on the very small adhesive thickness h_A. In fact, the results substantiated Eq. (6), and the generally accepted view of zero stress concentrations for identical adherends, and this allows the glue shear stress to be calculated very easily.

On the other hand, models C and D, for the wet/dry joint, did not produce a linear variation in $P_2(x)$ as shown in Figure 3(a). The corresponding adhesive shear stress is shown in Figure 3(b) where it is seen to vary from $0.1\sigma_0$ to $0.39\sigma_0$ whilst the shear stresses for Models A and B remain constant at $0.2\sigma_0$. Figure 4 shows how τ_A varies with scarf slope and, as one would expect, approaches

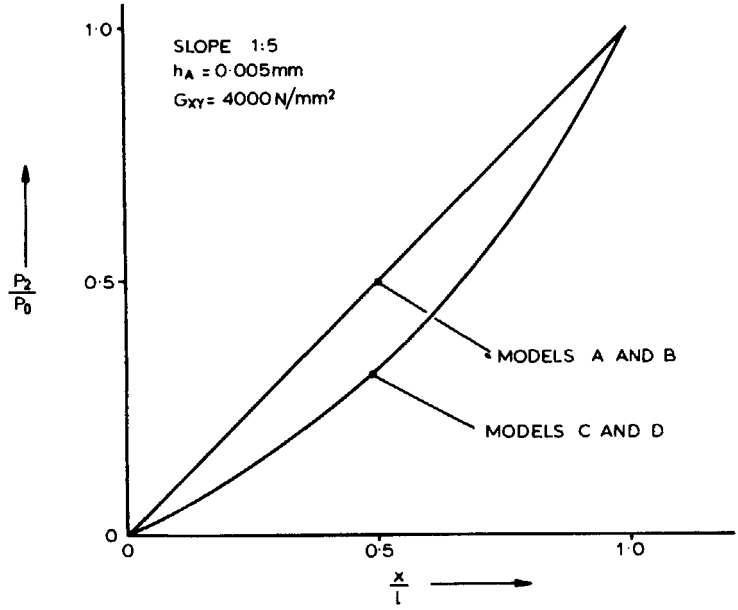

FIGURE 3(a) Variation of end load in material (2) with distance along joint.

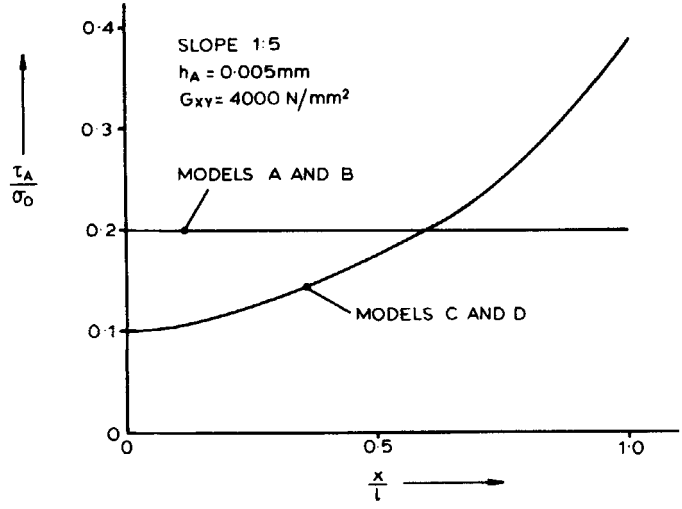

FIGURE 3(b) Variation of adhesive shear stress with distance along joint.

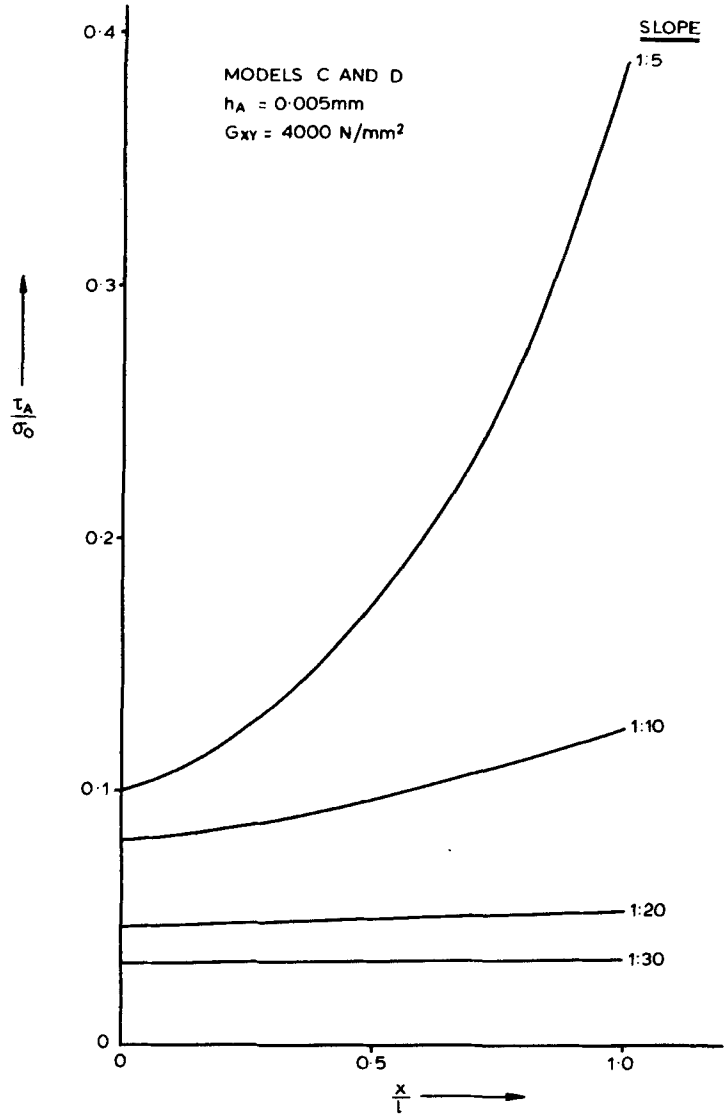

FIGURE 4 Variation of adhesive shear stress along joint for different scarf slopes.

uniform values as the slope is increased. For slopes smaller than 1 in 30, τ_A may be taken to be constant and it can then be calculated from Eq. (6).

The adhesive layer thickness, h_A, was difficult to assess in practice, but observations of a joint cross-section through a microscope showed that for machined dry/dry joints, this was in the region of 0.015 mm. For the wet/dry

joints, h_A could be smaller than this because the individual wet carbon fibres would be free to "sink" through the resin to make closer contact with the solid surface. Thus three different values were considered, namely 0.001, 0.005 and 0.05 mm. The effect of h_A on the adhesive shear stress is shown in Figure 5. For

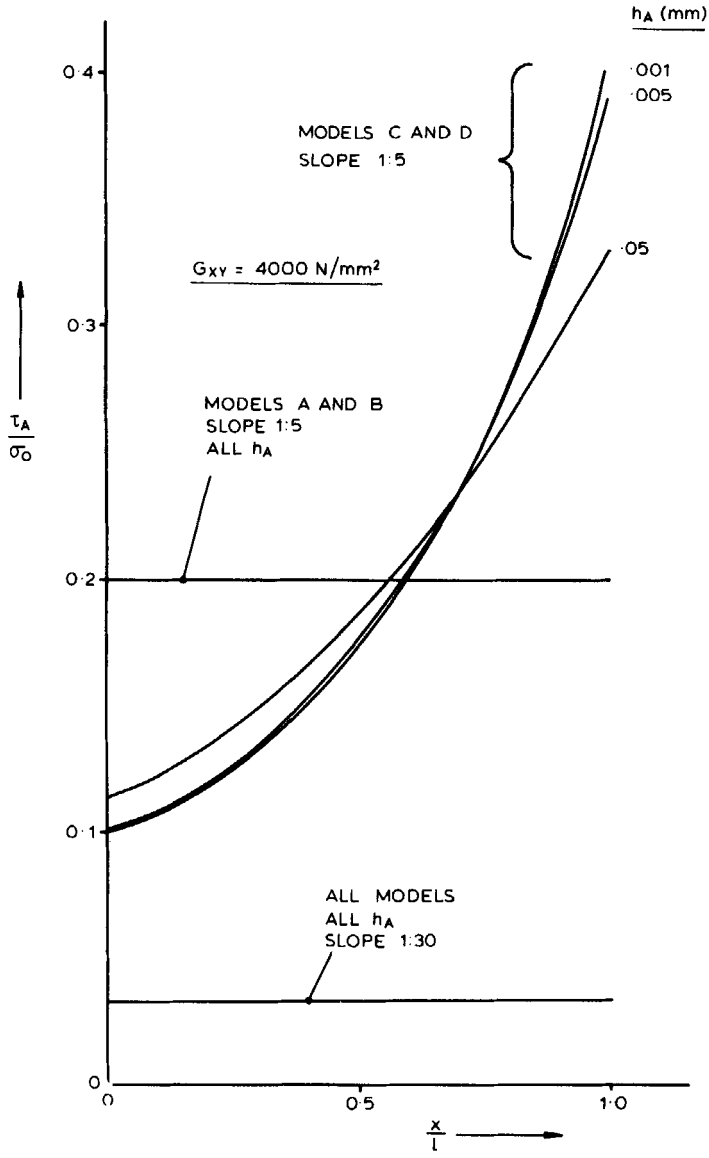

FIGURE 5 Effect of adhesive thickness on shear stress.

the large scarf slope of 1 : 5 it can be seen that h_A has a significant effect on τ_A for models C and D (the wet/dry joint) giving a much greater variation in τ_A for small h_A than for large h_A. However, models A and B (the dry/dry joint) are unaffected by h_A and this is also the case for all models for a scarf slope $\leqslant 1:30$.

The shear modulus, G_{XY}, for material (2) was also difficult to estimate, and so results were obtained for $G_{XY} = 2000$, 4000 and 6000 N/mm^2. The effect on τ_A is shown in Figure 6 where it is seen that the trend is similar to that obtained when h_A is varied (Figure 5). For a slope of 1 : 5, G_{XY} has a significant effect on τ_A giving relatively high values when $G_{XY} = 2000$ N/mm^2. However, for slopes $\leqslant 1:30$, τ_A is very nearly constant along the joint for all models and all G_{XY}.

4 EXPERIMENTS

4.1 Material properties

A number of unidirectional carbon fibre strips were supplied by Slingsby Engineering Ltd., and specimens were first cut from these strips to obtain some of the basic mechanical properties. Tension and compression testing in the fibre direction was carried out in accordance with the procedures laid down in Ref. 2. The carbon fibre used initially to make the strips was Courtauld's HTS sized Epikote 834 × 0.5% with a resin/carbon ratio of about 56% by weight. These strips were used throughout the tests, for materials (1) and (2) (Figure 1(b)) when making the dry/dry scarf joints and for material (1) only when making the wet/dry joints. For the latter case, material (2) was made up in the laboratories at Bristol University by passing five carbon fibre rovings through a bath containing Shell Epikure 113 and Epikote 162 resin, and then through a circular die to squeeze out the excess resin. Strips were made up by laying each major roving in a steel mould, being gently pressed into position by hand. When the required thickness of strip had been reached a steel plate was placed on the top surface in order to make this surface flat, but no pressure was applied. The material was allowed to dry before being removed from the mould and post-cured for eight hours at 55°C.

Table III gives mean values for Young's modulus in tension and compression, obtained from several identical tests. A certain amount of non-linearity was found in compression at high strain values, but this was not taken into account, and the E values quoted were obtained from initial slopes of the stress-strain curves. It is seen that the Slingsby and Bristol materials differ to some extent—the Bristol material being slightly more stiff than the Slingsby material, as well as having a high ILS (inter-laminar shear) stress value. This probably is an indication that the latter has more voids present than the former and certainly relatively large voids could be seen with the naked eye on machined surfaces.

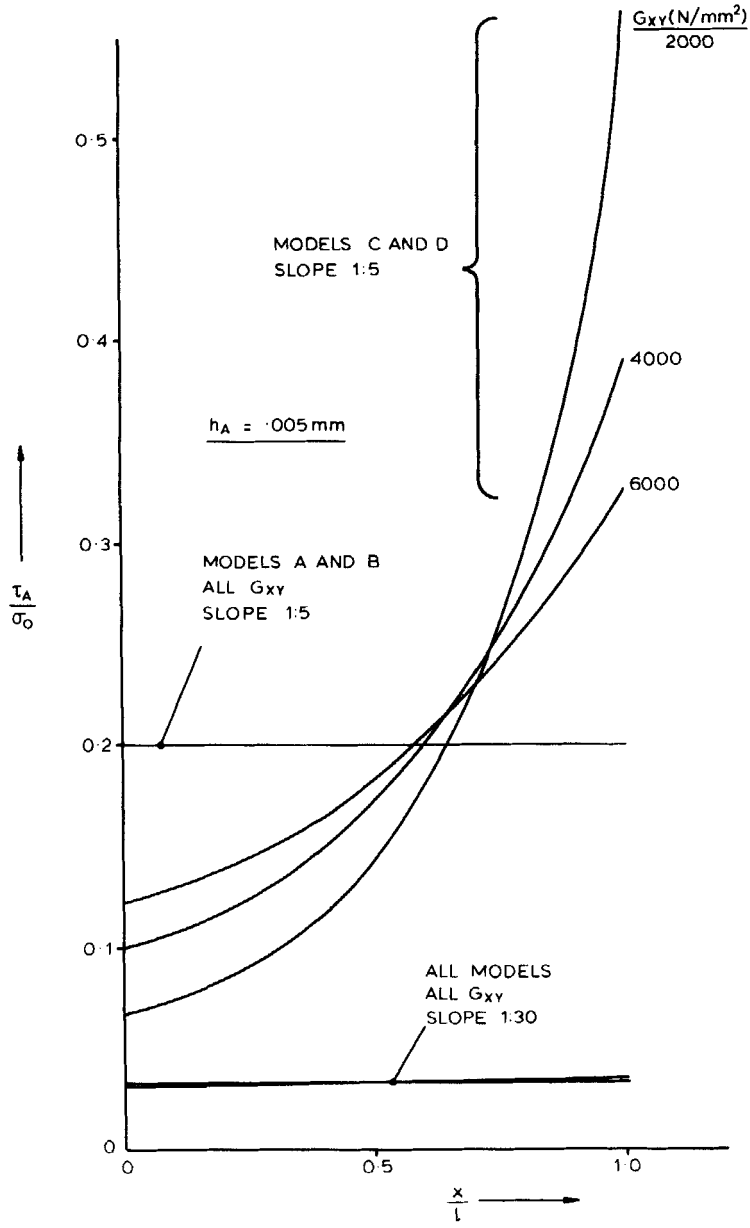

FIGURE 6 Effect of shear modulus on shear stress.

TABLE III

Unidirectional properties of CFRP (ILS—interlaminar shear strength)

	Slingsby material	Bristol material
E_X (tension)	109×10^3	125×10^3
E_X (compn.)	107×10^3	113×10^3
σ_{fail} (tension)	928	1172
σ_{fail} (compn.)	720	704
ILS	56.8	79.2

All dimensions N/mm^2.

By simply weighing the carbon fibre tows before and after the resin bath soak, there was evidence[7] to suggest that the resin/carbon ratio by weight was about 40% which is lower than that for the Slingsby material, and would account for the high modulus values. The value of $E_X = 108 \times 10^3$N/mm^2, used in Section 3 for the theoretical results, represents the mean tension and compression value for the Slingsby material.

4.2 Wet/Dry joints

The wet/dry joints were produced by forming scarf slopes on the Slingsby material and then laying in wet CFRP into the joint as shown in Figure 1(a). After the cure cycle, the joint cross-sections were machined to 10 mm (in width) × 3 mm (in depth) with a 40 mm central region (dimension d in Figure 1(a)). The ends of the completed strips were glued into cylindrical blocks made from aluminium alloy. Five scarf slopes were chosen, 1 : 20, 1 : 35, 1 : 50, 1 : 65 and 1 : 80. The steeper angled joints were intended to fail in shear along the glue line. The variation of longitudinal strain along the joints was measured by means of strain gauges. The strain outputs were found to be linear with increasing applied load, and for all practical purposes there was found to be no strain variation along the lengths of the joints. This means, of course, that the direct stress is constant and that the end load variation $P_2(x)$ is linear with x as predicted by theory. Table IV summarises the results at failure for the wet/dry specimens, where it can be seen that the joints with steep slopes (1 : 20 and 1 : 35) failed due to adhesive failure whilst the joints with lower slopes failed in the CFRP. It is difficult to say precisely how this CFRP failure occurred, as the process happened fairly quickly over a period of seconds, with audible cracking. As the failure load was approached, there was evidence of longitudinal splitting along the laid-in tows of the repair material, and on some occasions, strips of repair material which might have been individual rovings, became completely detached. Plate I shows a good example of this type of failure mechanism which is most probably caused by the interlaminar

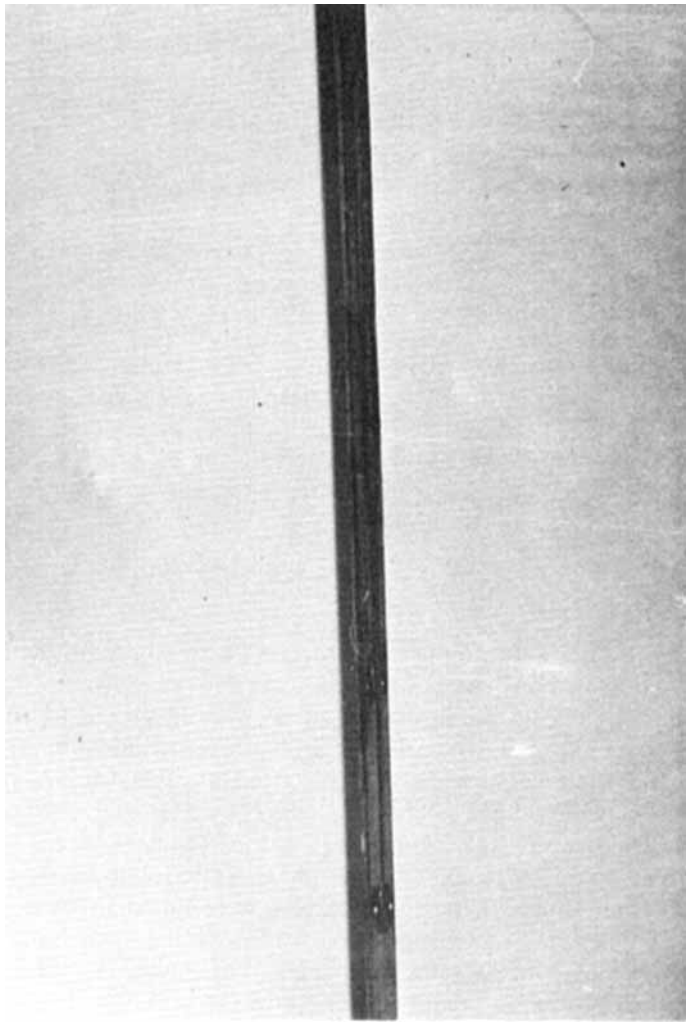

PLATE I Partial failure of wet/dry joint showing longitudinal separation of fibres.

shear stresses acting between the bond surfaces of the tows. Inspection after failure indicated that the carbon fibres had broken across various transverse planes in the tip regions and that this had then been followed by a cleaner shear failure of the adhesive layer. The broken pieces from two specimens (1 : 20 and 1 : 50 slopes) are clearly seen in Plate II, where the two different types of failure surfaces are evident. Table 4 shows, as expected, that the joints with low scarf slopes (1 : 50, 1 : 65 and 1 : 80) are much more efficient than those with high

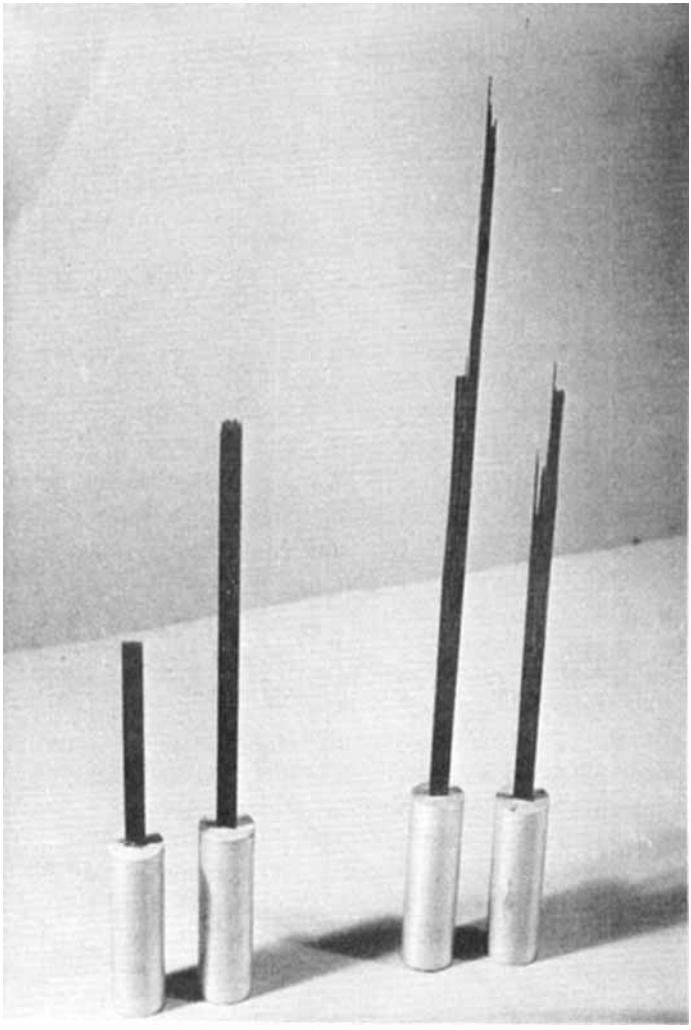

PLATE II Complete failure: two wet/dry joints.
L.H. specimen (1 : 20) shows clean fracture of adhesive layer.
R.H. specimen (1 : 50) shows longitudinal fibre splitting and adhesive layer fracture.

slopes, although it does not seem possible to get beyond 77% efficiency. Indeed, once an efficiency in this region had been reached, it was not possible to advance beyond it simply by decreasing the slope. This shows that the failure load, in these cases, was not dependent on the adhesive shear stress but on the strength characteristics of the in-laid repair material.

One other factor which should be taken into account at this point, is the

TABLE IV

Failure results for wet/dry joints

Scarf slope	Failure load (kN)	Failure stress (N/mm^2)	Tensile efficiency†	Adhesive shear stress at failure (N/mm^2)	Shear efficiency‡	Type of failure
1:20	11.95	398	43%	19.9	133%	adhesive
1:35	12.00	400	43%	11.43	76%	adhesive
1:50	21.50	717	77%	14.33	—	CFRP
1:65	17.90	597	64%	9.18	—	CFRP
1:80	18.00	600	65%	7.5		CFRP

† Based on 928 N/mm^2.
‡ Based on 15 N/mm^2.

effect that the inclined fibres have on the longitudinal strength of the inlaid material. It is well known that the tensile strength drops off rapidly as the fibre angle is increased, and Figure 7 shows this variation for a unidirectional thin laminate. The curve shown was obtained from Tsai and Azzi's failure criterion,[8]

$$\cos^4 \alpha + \left(\frac{X^2}{S^2} - 1\right) \cos^2 \alpha \sin^2 \alpha + \frac{X^2}{Y^2} \sin^4 \alpha = \frac{X^2}{\sigma_x^2} \tag{29}$$

In this Eq., X, Y and S are the strengths in the fibre direction, the transverse direction and that associated with shear in these two directions, respectively. The value for X was taken as 928 N/mm^2, and Y (= 70 N/mm^2) and S (= 90 N/mm^2) were obtained[9] for a well produced material, and therefore are probably high when used for the present repair material. It is seen that between 0° and 3° the axial strength drops to 88% of its base value. However, if Y and S are reduced to 35 and 45 N/mm^2 respectively, the strength at 3° is decreased to 68% of its base value. This corresponds to slopes up to 1 : 19 and is certainly another factor which makes the wet/dry joint less attractive than the dry/dry joint. Of course, Eq. (29) is for a thin laminate in plane stress, and this only approximates to the wet/dry joint which has a significant dimension in the z-wise direction. This effect can be taken into account by calculating σ_{z_2} from Eqs (18) and (16) for the unrestrained case, and by using $\varepsilon_{z_1} = \varepsilon_{z_2} = 0$ for the restrained case. The former case is probably more realistic, and using the values for the mechanical constants given in Section 3 we find that

$$\left(\frac{\sigma_{z_2}}{\sigma_{x_0}}\right)_{\max} = 0.3 \sin^2 \alpha - 0.024(1 - \cos^2 \alpha) \tag{30}$$

for the case when $\sigma_{x_1} = \sigma_{x_2} = \sigma_0$ at small angles.

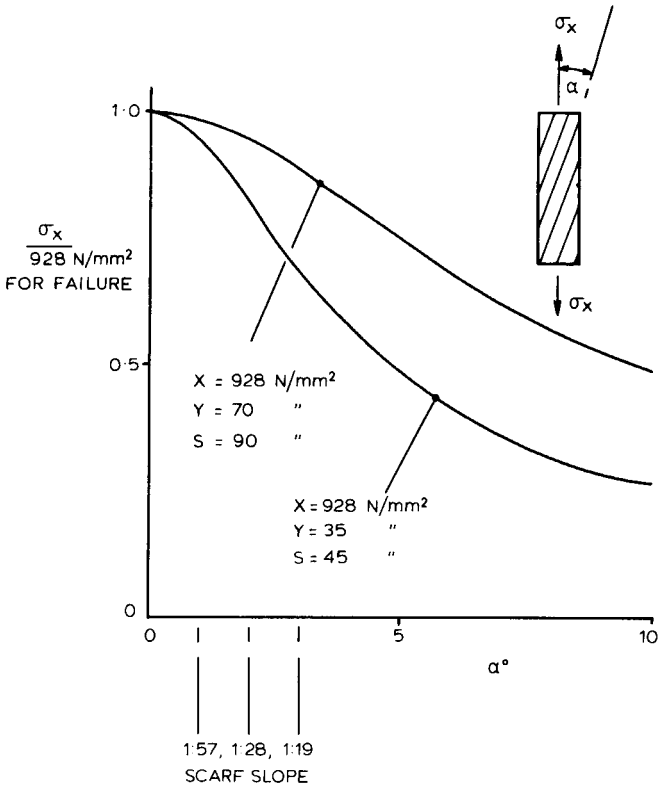

FIGURE 7 Tensile strength variation with scarf angle.

When $\alpha = 3^\circ$, we obtain

$$\left(\frac{\sigma_{z_2}}{\sigma_{x_0}}\right)_{\max} = \frac{7.56}{10^4}$$

which is very small indeed compared with the tensile strength in the z direction and can therefore be neglected. Even so, the results obtained from Eq. (29) show that the value of the scarf angle, α, is very important from the point of view of axial strength, and due care should be taken during the wet lay-up stage to ensure that all tows are straight and are laid at a uniform angle to the longitudinal axis.

The results for the two joints with high slopes (Table IV) were disappointing in as much as they both failed at the same load giving very different adhesive failure shear stresses. This can only be attributed to variations in this intrinsic property and must depend, to a large extent, on the method of joint manufacture. This is a worrying feature of the results, and points to the use of

large factors of safety on adhesive strength data. It should be mentioned here, that possibly higher joint efficiencies would have been obtained if some degree of consolidating pressure (such as that given by a vacuum bag) had been applied to the wet-laid material during manufacture. But even so, this might then not have been representative of a real sailplane repair, where it might not be physically possible to compact the joint in this way.

4.3 Dry/Dry joints

The dry/dry joints were made entirely from the Slingsby material. The first joint tested had a slope of 1 : 55 and was produced by surface grinding the slopes to a very high degree of accuracy. The dry scarf surfaces were stuck together using the same resin system (Epikure 113 and Epikote 162) as was used to make the repair material for the wet/dry joints, and a small consolidating pressure was applied. Longitudinal strain gauges gave a linear response to the applied tensile load and showed quite clearly that the strain was constant along the joint, thereby confirming the theoretical analysis. This particular specimen, surprisingly, reached a load of 37 kN (1193 N/mm^2) giving a stress which exceeded the nominal failure stress of 928 N/mm^2 for the Slingsby material. However, as the failure load was approached longitudinal splitting was extensive along the whole length and the specimen failed in the same way as the wet/dry specimens.

Six additional dry/dry joints were made up with the use of a hand-held electrical circular sander for rough shaping, and a hand-held plane fine sander for final shaping. This was thought to be more representative of the methods used in actual repair schemes. Unlike the wet/dry joint, only one scarf slope was used. Furthermore, the specimens were of uniform rectangular shape (nominally 10 mm × 4 mm) along their lengths, and the end supports were in the form of simple flat strips of soft aluminium alloy. This very much simplified the method of manufacture compared with the wet/dry specimens, and, in fact, did not lead to premature failure of the specimens. Table V gives the full set of results for the dry/dry joints. The cross-sectional area varied from one specimen to another so the failure stresses are not directly proportional to the failure loads. The two sets of bracketed joints indicate that two results had been obtained for the same specimen; after the first failure, the joint was re-assembled and re-tested, since for the 1 : 50 slope it was thought that a failure load somewhat higher than 27 kN should have been obtained, but as can be seen, this load was approximately confirmed with the second test. In the case of the 1 : 72 slope, the low failure load in the first test was caused by poor adhesion, as confirmed by the second test. The table shows quite clearly that up to slopes of 1 : 50 the joints fail in the adhesive layer whilst at higher slopes (ignoring the first 1 : 72 result) the failure mechanism is more complicated and

TABLE V

Failure results for dry/dry joints

Scarf slope	Failure load (kN)	Failure stress (N/mm^2)	Tensile efficiency†	Adhesive shear stress at failure (N/mm^2)	Shear efficiency‡	Type of failure
1:29	18	450	48%	15.5	103%	adhesive
1:40	25	618	67%	15.4	103%	adhesive
1:50	27	667	72%	13.3	89%	adhesive
1:50	30	741	80%	14.8	99%	adhesive
1:58	39	968	104%	16.7	—	CFRP
1:72	18	488	53%	6.8	45%	adhesive
1:72	36	976	105%	13.6	—	CFRP
1:83	36	972	105%	11.7	—	CFRP
1:55 (machined)	37	1193	128%	21.7	—	CFRP

† Based on 928 N/mm^2.

‡ Based on 15 N/mm^2.

involves longitudinal fibre splitting, CRFP transverse tensile fracture and adhesive failure, much in the same way as the wet/dry joints. However, comparing Tables IV and V shows that for the dry/dry joints, efficiencies in the region of 100% can be obtained whilst for the wet/dry joints this figure is much lower, at about 65%.

It is rather surprising that the dry/dry joint efficiencies should be as high as 100%+ when based on a tensile failure stress of 928 N/mm^2. This failure stress was obtained from relatively small specimens which measured approximately 5 mm × 1 mm compared with the joint specimens which measured about 10 mm × 4 mm. Thus the presence of large voids in the material would have had a greater effect on the former specimens than on the latter. Tensile tests on straight continuous strips (10 mm × 4 mm) showed that it was possible for this material to reach failure stresses of 1075 N/mm^2, and this would then have had the effect of reducing the joint efficiencies shown in Table V to below 100%. The adhesive shear stresses are also shown in this table, and it appears from the results for the higher hand-made slopes, that a maximum value in the region of 15 N/mm^2 can be expected. The results also confirm the fact that there is no point in reducing the slope beyond a value which allows the full tensile stress to be developed in the CFRP. In this case, this value would be about 1:65.

5 CONCLUSIONS

5.1 Theory

Various theoretical models have been developed to establish the stresses in scarf joints. Two types of joints were considered, namely a dry/dry joint in

which the fibres in both the repair and original material were in the same longitudinal direction, and a wet/dry joint in which the fibres in the repair material were laid along the scarf slope of the original material. The assumptions, on the one hand, of zero resultant transverse load and on the other hand of zero transverse strain resulted in the same governing equation for the dry/dry joint, but gave different algebraic expressions for the wet/dry joint; even so the corresponding numerical results gave stresses which, for all practical purposes, were identical. It may be concluded, then, that for the range of parameters investigated, either the zero transverse load model or the zero transverse strain model may be used.

For the dry/dry joints, the numerical results showed that the variation of the end load (in both the repair and original material) along the joint, was always linear, for all scarf angles. This gave rise, always, to a uniform shear stress in the adhesive layer. The results for the wet/dry joint showed that a uniform shear stress could only be obtained for small scarf angles (less than a slope of 1 : 30). The effect of varying the adhesive thickness and material shear modulus was studied, and this was found to be significant only at relatively large scarf angles. As a general ruling, which applies to both types of joints, the shear stress may be taken to be uniform in the adhesive layer for slopes less than 1 : 30 and may be calculated from the simple Eq.

$$\tau_A = \sigma_0 \sin \alpha \cos \alpha$$

The corresponding direct stress in the repair and original material may also be taken to be constant along the joint length and would equal σ_0.

5.2 Experiments

Tests on both wet/dry and dry/dry joints for slopes ranging between 1 : 20 and 1 : 83 supported the main theoretical conclusion of a linear variation in end load along the joint. For slopes greater than about 1 : 50 it was found that the joints generally failed suddenly in the adhesive layer. For smaller slopes the failure mechanism was more complicated with longitudinal fibre splitting, transverse tensile failure in the tip regions, and adhesive shear failure. For the wet/dry joints, longitudinal splitting was severe with sometimes large fingers of CFRP becoming detached as the failure load was approached, giving maximum joint efficiencies in the region of 65%. Much higher efficiencies were obtained with the dry/dry joints (in the region of 90%, based on a CFRP failure stress of 1075 N/mm^2) and this type of joint is recommended rather than the wet/dry joint.

Acknowledgements

Thanks are due to Messrs. N. A. D. Murphy and M. G. Thornton for developing the computer program, the production of the numerical results, and for testing the joints. Also to the British Gliding Association for financial assistance.

References

1. H. A. Perry, *Adhesive Bonding of Reinforced Plastics* (McGraw-Hill, NY, 1959), Chapter 2.
2. A. K. Ditcher and J. P. H. Webber, *J. Strain Analysis* **14,** 149–156 (1979).
3. F. Erdogan and M. Ratwani, *J. Comp. Mats.* **5,** 378–393 (1971).
4. S. G. Lekhnitski, *Theory of Elasticity of an Anisotropic Elastic Body* (Holden-Day, 1963), Chapter 1, Section 6.
5. L. Fox, *The Numerical Solution of Two-point Boundary Problems in Ordinary Differential Equations* (Oxford University Press, 1957).
6. F. Thamm, *J. Adhesion* **7,** 301–309 (1976).
7. N. A. D. Murphy and M. G. Thornton, *Scarf Joints in Unidirectional Carbon Fibre Reinforced Plastics.* Dept. of Aero. Eng., University of Bristol. Report No. 258, June 1980.
8. S. W. Tsai and V. D. Azzi, *AIAA Journal* **4,** 2 (1966).
9. A. K. Ditcher, F. E. Rhodes and J. P. H. Webber, *J. Strain Analysis* **16,** 43–51 (1981).